Regular Article

PHYSICAL CHEMISTRY RESEARCH
Published by the
Iranian Chemical Society
www.physchemres.org
info@physchemres.org

***Phys. Chem. Res.**, Vol. 6, No. 1, 31-43, March 2018*
DOI: 10.22036/pcr.2017.89007.1388

Interaction of HCN Molecule with the Pristine and Al, S and Al & S Doped Beryllium Oxide Nanotube: A Computational Study

M. Rezaei-Sameti* and H.J. Behbahani

Department of Applied Chemistry, Faculty of Science, Malayer University, Malayer, 65174, Iran

(Received 10 June 2017, Accepted 4 September 2017)

In this research, the effects of Al, S and Al & S atoms doped on the HCN interaction with beryllium oxide nanotube (BeONTs) are investigated by using density functional theory at the cam-B3LYP/6-31G(d) level of theory. Inspection of computational results reveals that the adsorption energies of all considered models are in the range of -1.39 to -31.84 Kcal mol^{-1} and exothermic in view of thermodynamic approach. Due to doping Al and Al & S atoms, the adsorption energy, and the gap energy of BeONTs/HCN complex alter significantly from the original values, and so the conductivity and activity of the nanotube increase significantly from the original values. The natural bonding orbital (NBO), and molecular electrostic potential (MEP) results demonstrate that the HCN molecule has a donor electron effect. The computational results indicate that doping of Al, S and Al & S increase the sensivity of the BeONTs to detect and adsorb the HCN molecule.

Keywords: BeONTs, Al & S doped, HCN adsorption, DFT, MEP, NBO

INTRODUCTION

In recent years a novel nano materials including nanoparticle, nano clusters, nanotubes, nanoplat, and nanowires have attracted considerable interest due to their special structural, thermal, mechanical, optical and electrical properties. These novel materials have a wide range of application in nano sensor, nano electronics, storage of fuels, and removal of hazardous pollutants, nano drug delivery, and nano filter for poisonous substance [1-6].

Hydrogen cyanide (HCN) is one of the poisonous and pollutant compounds and extremely harmful to the human body and environmental systems, because it inhibits cellular oxidative processes. It is commonly used in chemical warfare agents known as blood agents. In the recent years, detecting, monitoring and adsorbing hydrogen cyanide in the air and environmental system require a sensitive, reliable, and specific method [7-12].

For this purpose, the extensive studies have been carried out on the detecting and adsorbing HCN gas by nano materials. Zhang *et al.* [3], Bahestein *et al.* [13], Ahmadi Peyghan *et al.* [14] and Srivastava *et al.* [15] showed that the pristine CNTs, AlNNTs and BC2NNT can weakly adsorb HCN molecule. Whereas, Zhao *et al.* [12] and Marvi *et al.* [10] demonstrate that HCN molecule can be adsorbed on the surface of graphene with oxygen-containing group and on the external surface of the BeONTs. The recent theoretical and experimental research about beryllium oxide nanotube [16-19] reveal that this nanotube has the remarkable structural, optical, electrical, thermal and mechanical properties. The large iconicity of the beryllium and oxygen bonds and its large gap energy make the beryllium oxide nanotubes proper materials to be widely used in the electronics industry and nano-filters [20-23].

Following our previous research on the electrical and structural properties of doping and adsorbing BPNTs, AlNNTs and AlPNTs [24-27], in this research, we investigate the capability of the pristine and Al, S and Al&S doped BeONTs for adsorbing or detecting HCN molecule. Up to now, no experimental or theoretical investigations

*Corresponding author. E-mail: mrsameti@malayeru.ac.ir

have been reported on the adsorption of the HCN gas on the Al, S, and Al & S doped BeONTs surfaces. At the first step of this research, we consider different orientations and configurations for the HCN adsorption on the exterior and interior surface of nanotube, and then all models are optimized at the B3LYP/3-21G level of theory. The sixteen stable configuration models for HCN/BeONTs complexes are selected and named with the AI to DIV models (see Fig. 1). The A and B models are used to denote the vertical adsorption HCN gas from N and H atom on the exterior surface of nanotube, respectively. The C and D models are used to denote the horizontal adsorption of HCN gas from C atom on the exterior and interior surface of the nanotube, respectively. In each model, the indexes I, II, III and IV are applied for pristine, Al, S and Al&S-doped, respectively.

However, the reason for the selection of aluminum and sulfur atoms in this project is that Al atom has three electrons in its valence layer while beryllium atom has two electrons, and this additional electron of Al atom changes the electrical behavior of the BeONTs. On the other hand, the sulfur atom has a larger radius than the oxygen atom of the nanotubes, which can also change the electrical and structural behavior of the nanotubes.

The structure and electrical properties, adsorption energy, highest occupied molecular orbital (HOMO) and lowest unoccupied molecular orbital (LUMO) parameters, the quantum molecular descriptors, density of state (DOS), NBO and MEP plots for all adsorption models from AI to DIV are calculated by using DFT method. The results of this research may be useful for making a sensor or adsorbent of HCN molecule.

COMPUTATIONAL METHODS

The structures of the AI to DIV presented models are individually optimized by using DFT methods at the cam-B3LYP/6-31G(d) level of theory [28] embedded in GAMESS suite of program codes [29]. After the optimization, the adsorption energy (E_{ads}) of HCN gas on the surface of pristine, Al, S and AlS doped BeONTs is calculated as follows:

$$E_{ads} = E_{BeONTs/HCN} - (E_{BeONTs} + E_{HCN}) \quad (1)$$

Here, $E_{BeONTs/HCN}$, E_{BeONTs} and E_{HCN} are obtained from the scan of the potential energy of the BeONTs/HCN complex, BeONTs and HCN respectively.

The gap energy (E_{gap}) , electro chemical potential (μ), global hardness (η), electronagivity of nanotube (χ), electrophilicity index (ω), global softness (S) and charge transfer parameters (ΔN) of the nanotubes are calculated by the Eqs. ((2)-(9)) [23,25,27].

$$Egap = E_{LUMO} - E_{HOMO} \quad (2)$$

$$\mu = -(I + A)/2 \quad (3)$$

$$\eta = (I - A)/2 \quad (5)$$

$$\chi = -\mu \quad (6)$$

$$\omega = \mu^2 / 2\eta \quad (7)$$

$$S = 1/2\eta \quad (8)$$

$$E_{FL} = (E_{HOMO} + E_{LUMO})/2 \quad (9)$$

$$\Delta N = (-\mu/\eta)$$

where I ($-E_{HOMO}$) is the ionization potential, and A ($-E_{LUMO}$) is the electron affinity of the molecule.

RESULTS AND DISCUSSION

The Structural and Geometrical Properties

The optimized structures of the AI to DIV models are shown in Fig. 1, and the geometrical parameters involving bond length, and bond angle are given in Table S1 in supplementary data. In the all adsorption models, the length and width of the nanotube is 5.86 and 9.43, respectively, and included 32 Be and 32 O atoms with chirality C1. Based on the results, it is found that the calculated mean Be-O bond length and mean O-Be-O or Be-O-Be bond angle of pristine BeONTs are 1.55 Å and 118°. This result is in agreement with other research results [20-22]. With doping Al, S and Al & S, the bond length of the neighbor of doping position increases significantly from 1.55 Å to 1.88, 2.02, and 2.06 Å, respectively. The investigated results show that with doping Al, S and Al & S atoms, the surface of the nanotubes is rippled, and the doped atom tends to the outer surface of the nanotube. Therefore, the total energy of the system reduces, because the electron-electron repulsion reduces, and this result is in agreement with the other research results [1,19-22]. According to the obtained

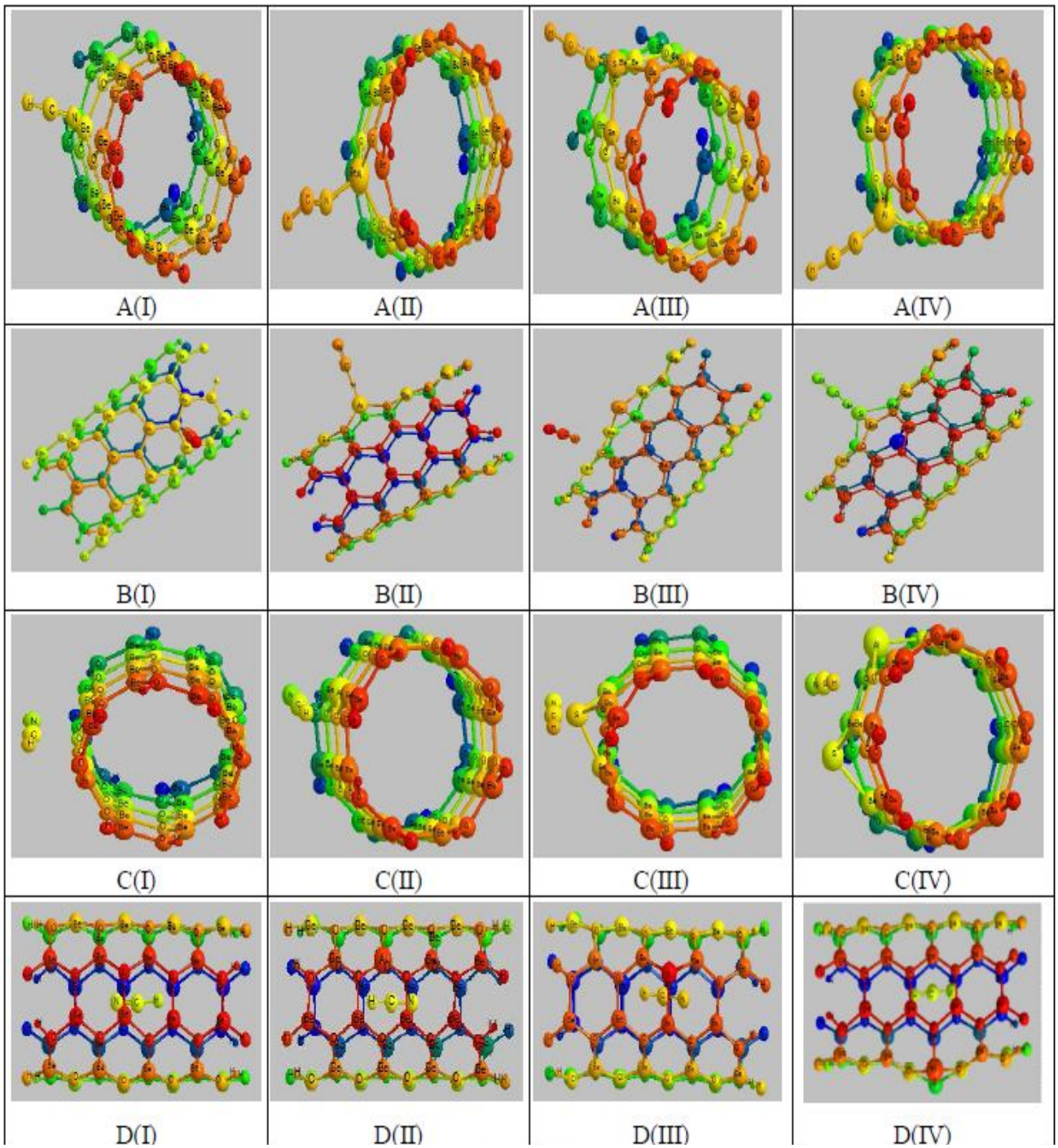

Fig. 1. 2D views of adsorption of the HCN gas on the surface of pristine and Al, S and AlS doped of (4,4) armchair model of BeONTs for (AI to DIV).

results, with doping Al, S and Al & S atoms, the bond angles of Be-O-Be decrease significantly from pristine model. The doping of Al, S and Al & S atoms causes that the hybridization of the Be atom in the nanotube changes from SP^2 to SP^3. On the other hand, when a HCN molecule is adsorbed on the surface of nanotube the Be-O bond length and Be-O-Be bond angle alter slightly from original values.

The results of adsorption energy, dipole moment of nanotube, NBO charge of HCN gas, and the distance between the HCN gas and nanotube are calculated from the optimized structures of the AI to DIV models and results are listed in Table 1. As we can see in Table 1, the adsorption energies of the AI-DIV models alter in a range from -1.39 to -31.84 kcal mol^{-1}. These results indicate that the HCN molecule can be physically adsorbed on the surface of the nanotube. The negative E_{ads} values in the AI to DIV models confirm that the adsorption process on the exterior and interior surface of nanotube is exothermic and favorable in view of thermodynamic approach. The adsorption energy values of the AII, AIV, CII, CIV, DII and DIV are -31.84, -31.28, -25.87, -31.3, -22.17 and -30.21 kcal mol^{-1}, respectively. The adsorption energy value of the AII model is more than that of the other models, and the distance between HCN gas and nanotube in this model is lower than that in other models. Comparison results demonstrate that with doping Al and Al & S atoms, the adsorption energy of HCN/BeONTs increases significantly from the pristine models. From adsorption energy result, we investigate the recovery time of nanotube sensor. Based on the conventional transition state theory, the recovery time of the nanotube sensor device is dependent to the adsorption energy: (see Eq. (10))

$$\tau = \nu_0^{-1} \exp^{(-Ead/kT)} \tag{10}$$

where T is temperature, k is the Boltzmann's constant, and ν_0 is the attempt frequency. According to Eq. (10), the more negative adsorption energy leads to an increment in the recovery time and the stronger interactions between nanotube and adsorbate.

However, as seen from Table 1, the adsorption energies of the AII model is more negative than other models and so the recovery time of this model is more than that of the other models. Therefore, the interaction of HCN gas with nanotube in the AII model is stronger than other models.

In the most stable configuration, A(II) model, the transferred charge from the HCN molecule toward the nanotube surface is about -0.8 |e|. It is notable that in the D(IV) model, which HCN molecule is adsorbed onto the inner surface of the nanotube, the adsorption energy and distance of HCN molecule from nanotube is -30.21 eV and 1.12 Å, respectively, and about 0.05 |e | charge is transferred from the nanotube surface to the HCN molecule. The calculated results demonstrate that the most charge transferred is about -0.80 |e| for the A(IV) models, from the HCN molecule towards the nanotube, and is about 0.98 |e| for the D(III) models, from the nanotube towards the HCN molecule. Whereas, the adsorption energy and charge transfer between HCN molecule of the BI model are lower than those of the other models, and the longest distance between nanotubes and HCN molecule occurs in this model, emphasizing that this configuration model is more unstable than other models.

To investigate the changes in the electronic properties of BeONTs, the NBO charge density on the Be and O atoms around doping and adsorbing position is calculated and results are given in Table 2. Inspection of results reveal that the charge density in the AI, AII, BI, BII, CI, CII, DI and DII models is positive for the beryllium atoms and is negative for the oxygen atoms. It is notable that the charge density of Be and O atoms in the B(II) model is more than that in the other models. On the other hand, with doping S atom, the charge density of Be and O atoms in the AIII, AIV, BIII, BIV, CIII, CIV, DIII and DIV models is lower than that in the other models. However, by substituting an oxygen atom with a sulfur atom in the nanotubes, evidently the NBO charge density of the beryllium and oxygen atoms is significantly altered, in a way that the charge sign in the beryllium and oxygen atoms changes to negative and positive, respectively.

HOMO and LUMO Descriptions

To study the electronic structures of the AI to DIV models, the frontier orbitals: the highest occupied molecular orbital (HOMO) and lowest unoccupied molecular orbital (LUMO) are calculated and the HOMO-LUMO plots for all adsorption models are displayed in Fig. 2.

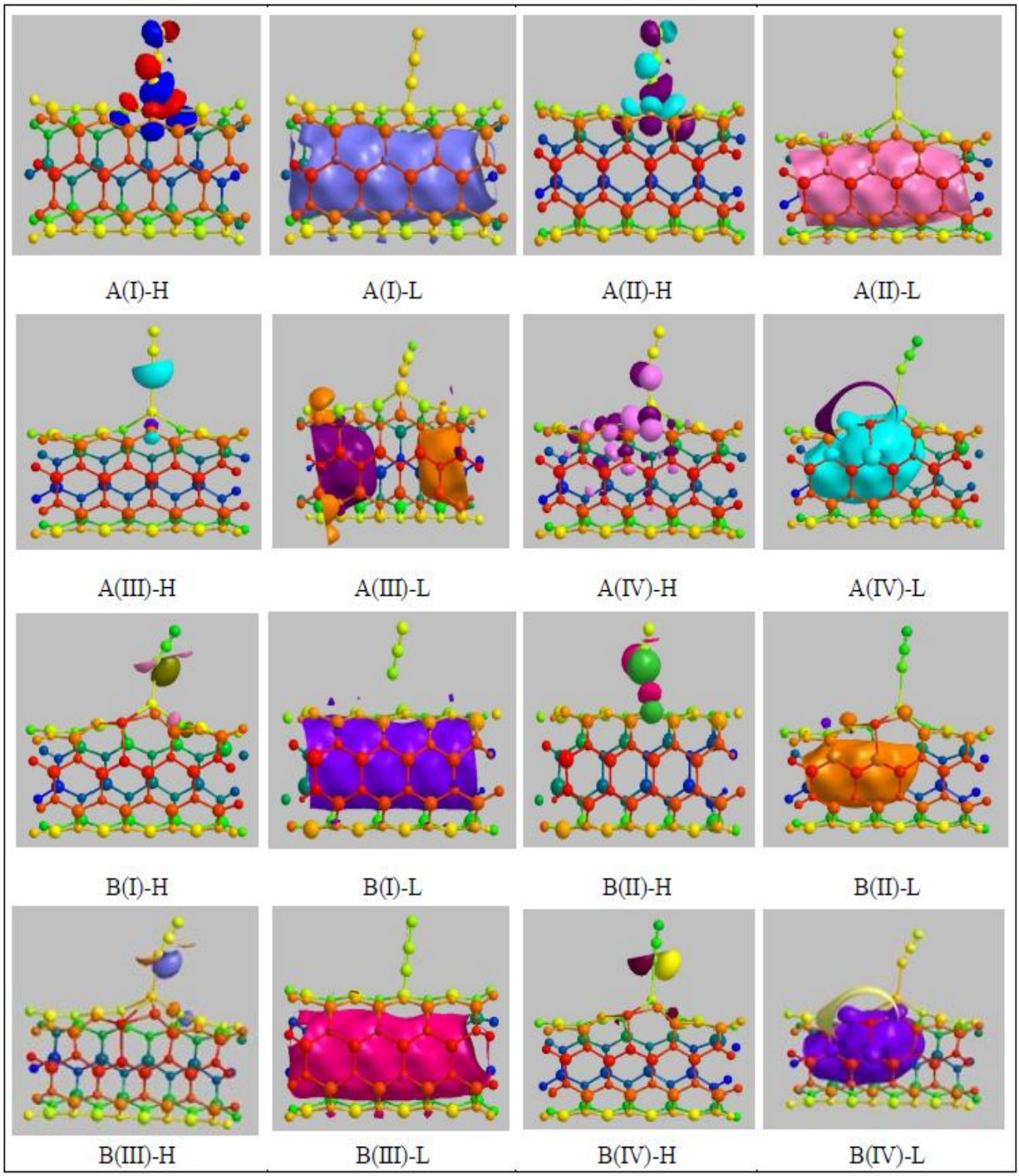

Fig. 2. Plots of HOMO and LUMO structures for HCN adsorption on the surface of pristine and Al, S and AlS doped of (4,4) armchair model of BeONTs for (AI to DIV).

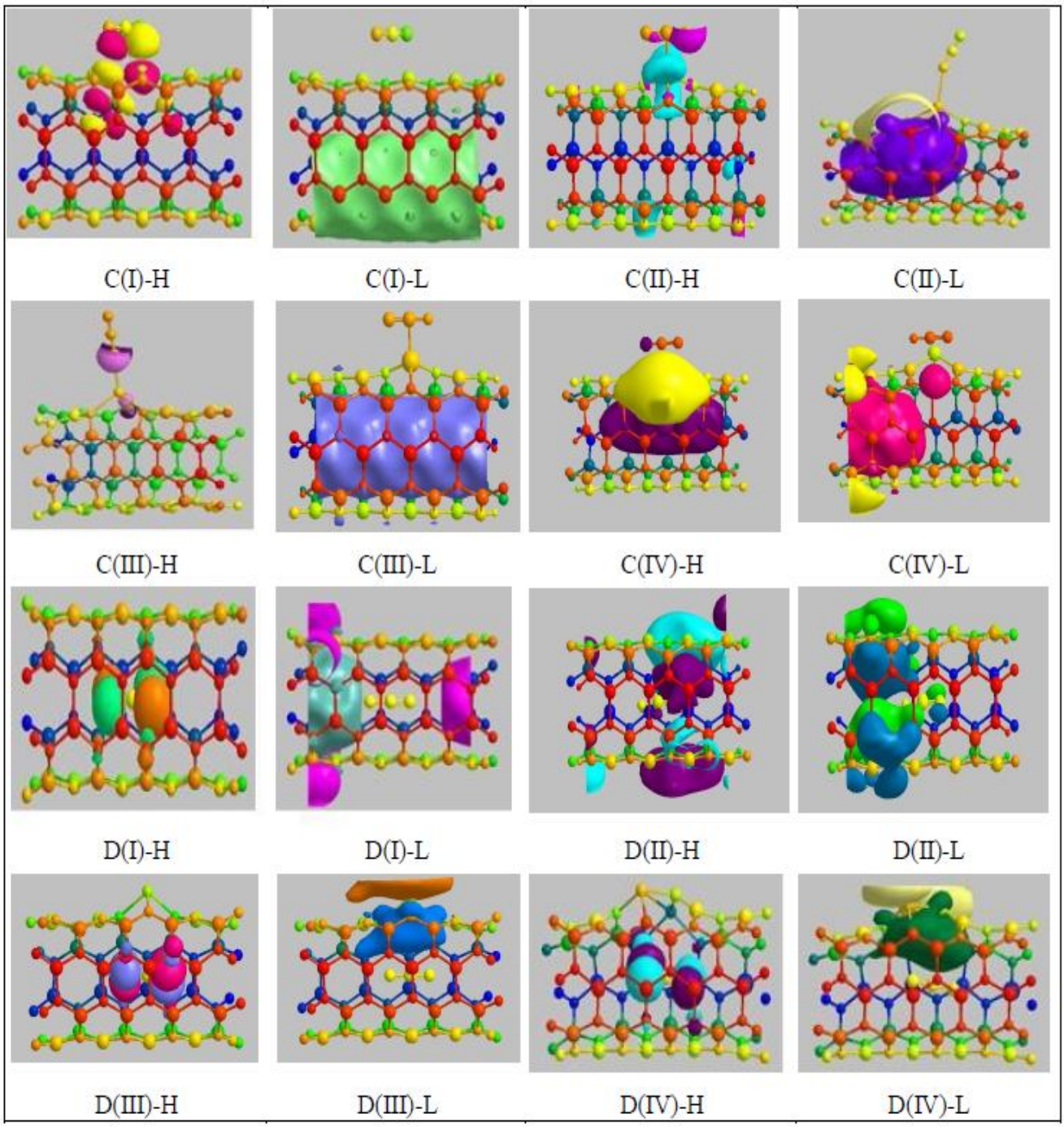

Fig. 2. Continued.

The HOMO densities for the AI to DIV adsorption models are localized around HCN molecule with most contributions around N atoms. These results confirm that the HCN molecule can be undergone an electrophilic attack. In contrast, the LUMO densities of the AI, AII, AIV, BI, BII, BIII, BIV, CI, CII and CIII adsorption models are distributed regularly inside of the nanotube. For the AIII, CIV, DI and DII adsorption models, the LUMO densities are localized at the inside of the nanotube, with the most contribution at the nanotube ends. On the other hand, for the DIII and DIV adsorption models the LUMO densities are localized inside of the nanotube around HCN adsorption position. Comparison of the charge distribution of HOMOs and LUMOs show that the electronic structure properties of the CIV, DI and DII models are more strongly influenced than those of the other models. Whereas, in all adsorption models, the HOMO density is localized on the surface of the HCN molecule and the LUMO density is localized on the surface of nanotube, suggesting that in these complexes HCN molecule is an electron donor species and the nanotube is an electron acceptor one. This result suggests a charge transfer from the HOMO to the LUMO.

To better understand the nature of the interaction of HCN molecule with nanotube, we calculate the gap energy (E_{gap}) between HOMO and LUMO levels, electronic chemical potential (μ), global hardness (η), electrophilicity index (ω), electronegativity (χ) and other quantum descriptors of the nanotubes by using Eqs. ((2)-(9)), and the calculated results before and after HCN adsorption are given in Table 3 and Table S2 in supplementary data.

It can be found from Table S2 in supplementary data that with doping of Al and Al & S atoms (in the II and IV models) the HOMO and LUMO orbitals split to α and β spin. The gap energy for α spin adsorption models is in range of 3.43 to 5.01 eV, whereas these values for β spin are in range of 5.44 to 6.71 eV. These results demonstrate that HCN adsorption on the Al and Al & S doped has more influence on the energy gap of the nanotube than the pristine nanotube. The E_{gap} describes electrical transport properties in nanotube and it is a measure of electron conductivity. It is well known that nanotubes with high-energy gap are kinetically stable. The BIII model with high-energy gap 7.16 eV is more stable than other models. Moreover, the HCN adsorption on the nanotube surface leads to decrease in the E_{gap}, global hardness (η) and the electronic chemical potentials, while the global softness (S), charge transfer (ΔN) will be increased.

It is noticeable that at all adsorption models, due to high chemical potential of HCN molecule, a charge transfer takes place from HCN molecule toward outer surface of the BeONTs, thereby the stability between HCN and BeONTs decreases and their reactivity increases.

GaussSum program [30] has been used to obtain the density of state (DOS) plots. The DOS plots for all HCN/ BeONTs adsorption models are calculated in the range of -15 to 10 eV (see Fig. 3). The DOS plots display that with doping of Al and Al & S atoms and HCN adsorption, one peak appears near the valence and conduction level of the nanotube, and so the E_{gap} of nanotube reduces from original values. This phenomenon suggests that BeONTs would be a good candidate for detecting and adsorbing the HCN molecule.

To further study the susceptibility of BeONTs for adsorbing HCN molecule, the work function of systems for the charge transfer between HCN and the adsorbents are calculated. Theoretical studies have shown that approaching HCN molecule to the surface of nanotube might effectively modify the field emission property which is necessary to estimate the potential for designing efficient field emission display [31,32]. The emitted electron current densities in a vacuum are described by the following classical equation:

$$j = AT^2 \exp^{(-\Delta\phi/kT)} \quad (11)$$

where A is called the Richardson constant (A m^{-2}), T is the temperature (K) and $\Delta\Phi$ (eV) is the material's work function. The calculated results of work function and Fermi level energy demonstrate that at all adsorption models the Fermi level increases and the work function decreases. The decrement in the work function shows that the field emission properties of the BeONTs are facilitated with the HCN adsorption. Comparison results confirm that the AII, AIV, BII, BIV, CII, CIV, DII and DIV models are a good strategy for improving the sensitivity of BeONTs to toxic

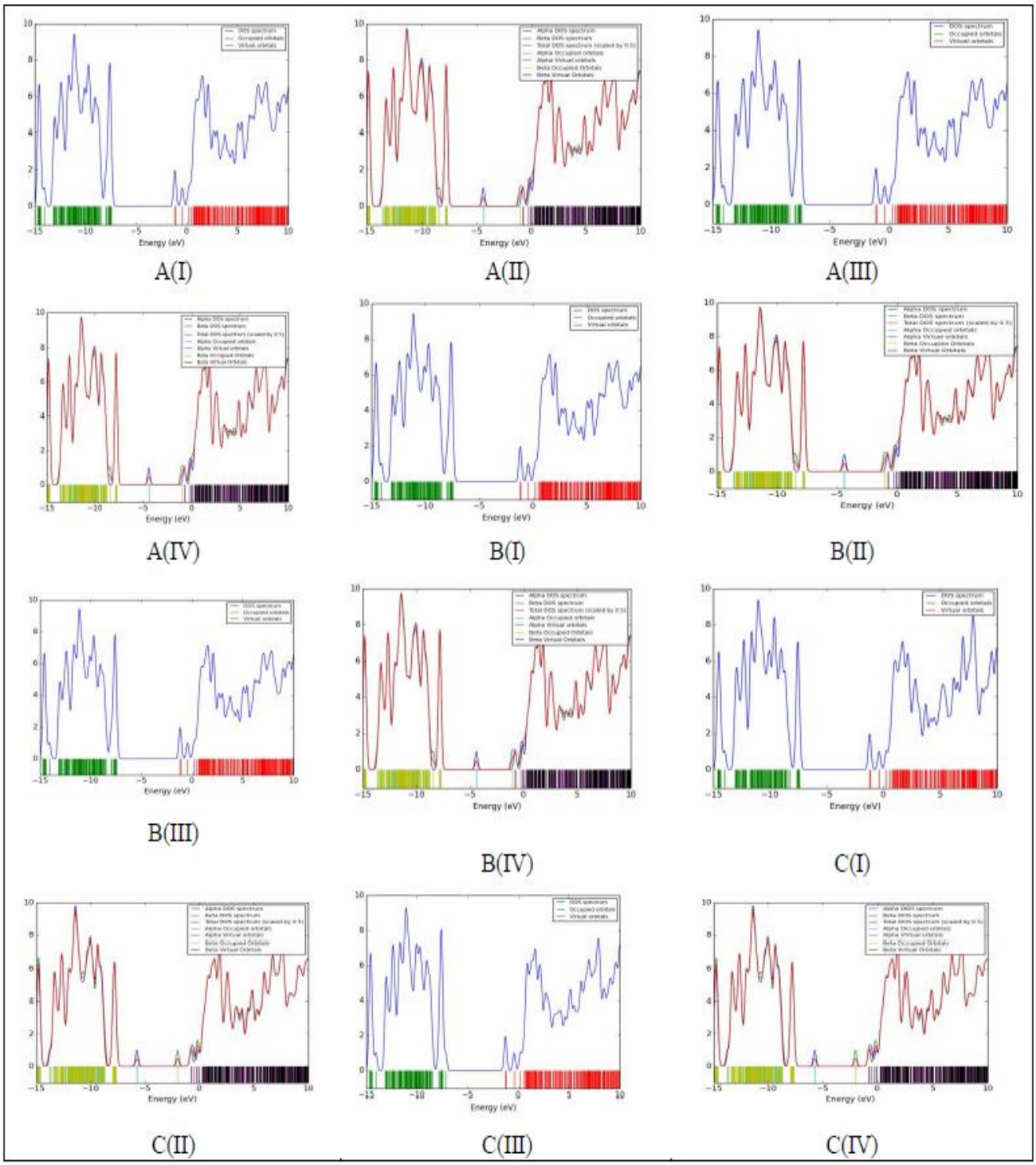

Fig. 3. DOS Plots for HCN adsorption on the surface of pristine and Al, S and AlS doped of (4,4) armchair model of BeONTs for (AI to DIV).

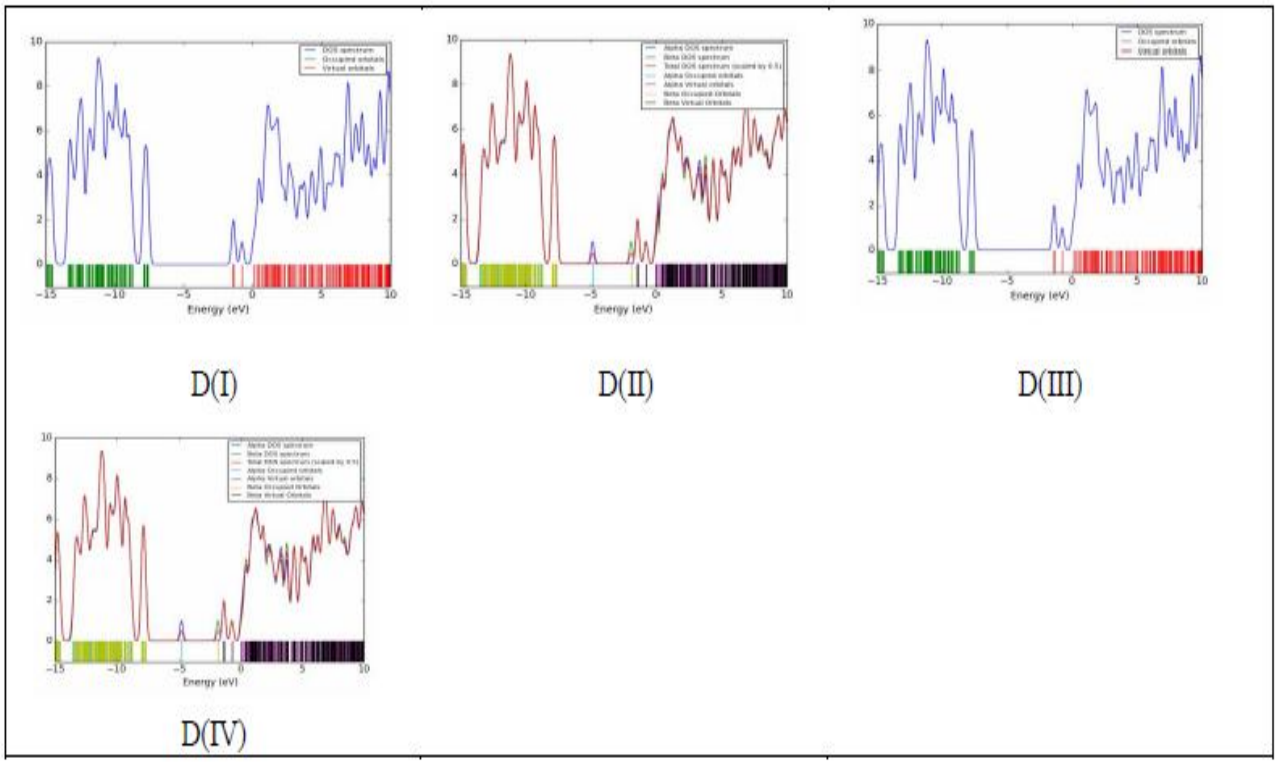

Fig. 3. Continued.

HCN molecule, which is in agreement with adsorption energy.

Molecular Electrostatic Potential (MEP)

To investigate the electrical properties and charge distribution around adsorption position, the molecular electrostatic potential (MEP) [33-35] is calculated for all AI to DIV models and results are shown in Fig. 4. In the MEP maps, the blue color represents the positive charges or the nucleophilic regions and the red color represents the negative charges or the electrophilic regions. It can be clearly observed that at all adsorption models there is a significant electron density, and negative potential, red color, above the adsorption position. The MEP maps of A, C and D models in the adsorption position of HCN/nanotube represent that the maximum positive electrostatic potential occurs over the N and C atoms of HCN and the maximum negative electrostatic potential (blue color) occurs at the end and opposite end regions of the nanotubes. On the other hand, in the B model, a strong positive electrostatic potential (blue color) and weak negative electrostatic potential (red color) occur at the surface of nanotube and HCN molecule, respectively, where the hydrogen atoms are located. As shown by the MEP map in Fig. 4, in the D models, the positive charge (blue colors) is localized on the inner layer of the nanotube, and negative charge (red color) is localized on the outer side of the nanotube. It indicates that a low charge transfer from the HCN molecule results in a weak ionic bonding in the surface of BeONTs. This result is in agreement with HOMO and LUMO results. Therefore, it is expected that with adsorption of HCN molecule the exterior layer of nanotube becomes rich of negative charge and interior layer of

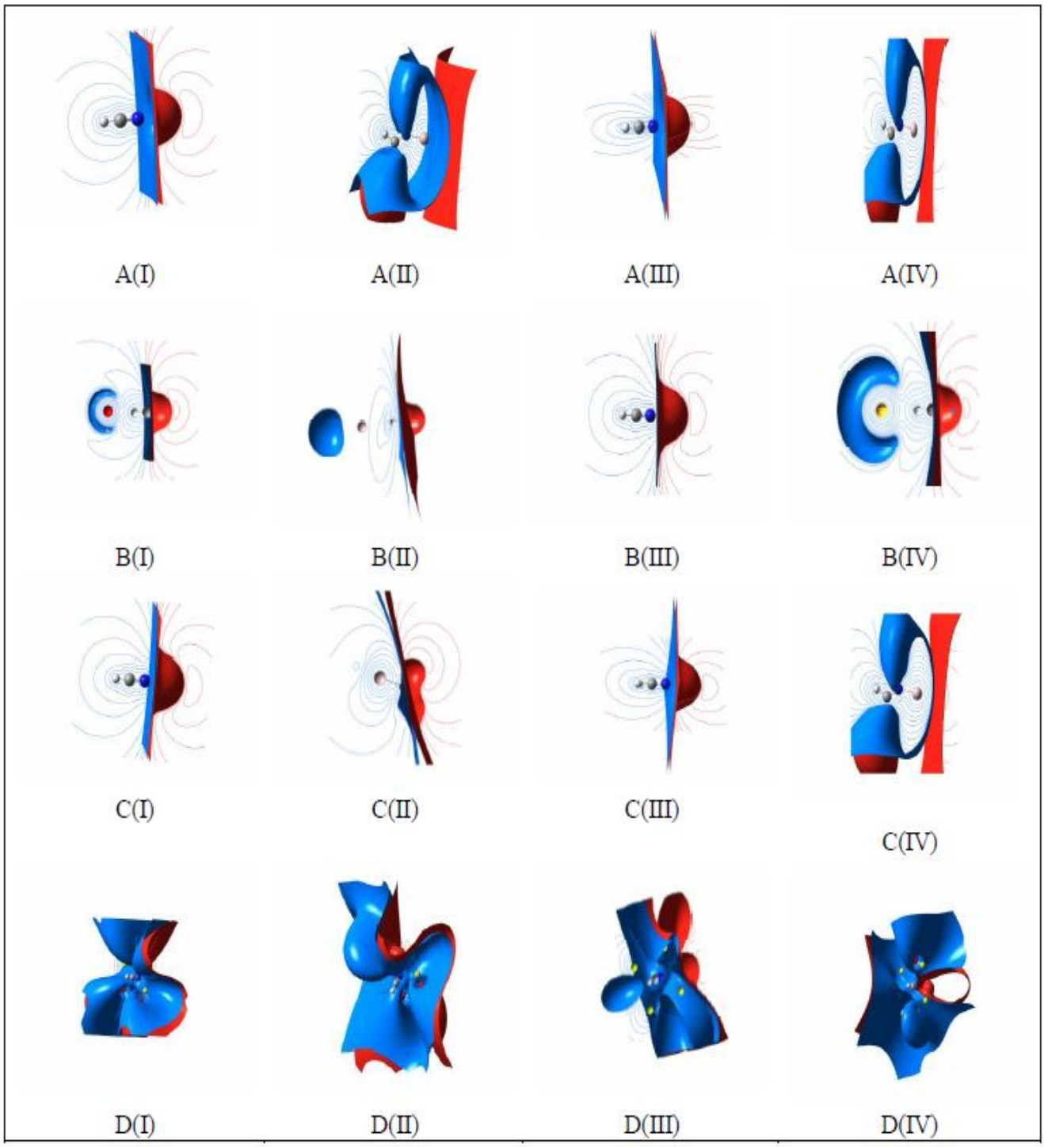

Fig. 4. MEP Plots for HCN adsorption on the surface of pristine and Al, S and AlS doped of (4,4) armchair model of BeONTs for (AI to DIV).

nanotube becomes poor of charge.

Natural Bond Orbital (NBO)

To further survey the interaction of HCN molecule with the pristine, Al, S, Al & S doped BeONTs, we focus on the NBO (natural bond orbital analysis) and stabilization energy $E^{(2)}$ that it is calculated from the second order perturbation theory analysis of the Fock-matrix. The stabilization energy $E^{(2)}$ is calculated by the Eq. (12) [36,37]

$$E^{(2)} = q_i \frac{F_{ij}^2}{\varepsilon_j - \varepsilon_i} \quad (12)$$

where q_i is donor orbital occupancy, ε_i and ε_j are orbital energies and F_{ij} is the off-diagonal NBO Fock matrix element. The electron donor orbital *i*, electron acceptor orbital *j*, and stabilization energy $E^{(2)}$ for all adsorption models are listed in Tables S3-S6 in supplementary data.

It can be seen that the estimated value of $E^{(2)}$ between donor- acceptor Lewis-type NBOs $\sigma Be52-O51 \rightarrow \sigma^* Be41-O51$ in the AI, AIII, BI, BIII, CI, CIII, DI, DIII models are more than other Be-O bonding to Be-O antibonding. In addition, in the BII, BIV and DIV models the $\sigma Be52-O51 \rightarrow n^* Al$ donor-acceptor orbital has the more stabilization energy $E^{(2)}$. For the CII and DII models, the AII and AIV models, and the CIV model the $\sigma Be22-O22 \rightarrow \sigma^* Be12-O11$, $\sigma C81-H83 \rightarrow \sigma^* Be41-N82$ and $\sigma C81-H83 \rightarrow \sigma^* Al63-N82$, as donor-acceptor NBOs, respectively, have the most important common interaction with the highest energy $E^{(2)}$. The calculated NBO results indicate that the $E^{(2)}$ values of Al doped BeONTs in the AII, BII, CII and DII models are lower than those in other models. So, doping Al atom reduces the stabilization energy between the donor and acceptor orbitals, while doping S atom increases this stabilization energy from the pristine states. These results display that the transition from donor orbital to acceptor orbital is dependent to the position of adsorbent and doping atom. It is notable that the doping impurity atoms in nanotube change significantly the $E^{(2)}$ values and charge transfer between donor and acceptor orbitals. The interactions of some molecular orbitals of the two constituents in the favorable adsorption systems with the largest $E^{(2)}$ values show the more intensive interaction between donor and acceptor bonding or antibonding orbitals considered.

CONCLUSIONS

In this research, we focused on the effects of Al, S, Al & S doped on the adsorption of HCN molecule on the surface of BeONTs. The calculated results demonstrate that the adsorption of HCN molecule on the surface of the pristine, Al, S, Al & S doped BeONTs is exothermic and favorable in view of the thermodynamic approach. Comparison results indicate that the adsorption energy of the Al, Al & S-doped BeONTs is more than that for other models, and therefore the adsorption of HCN molecule on the surface of Al, Al&S-doped models is more favorable than pristine and S doped. The HOMO-LUMO results reveal that in all adsorption models the density of HOMOs is localized on the surface of HCN molecule, and the density of LUMOs is distributed around nanotube. The NBO and MEP results indicate that the HCN molecule can undergo an electrophilic attack and indicate that electrons transfer from HCN molecule to nanotube surface. On the other hand, with adsorption of HCN molecule, the gap energy, global hardness, and electronic potential of HCN/BeONT complex alter significantly from the original state.

ACKNOWLEDGMENTS

The author thanks from the information technology centre Malayer Universities for supporting this research.

SUPPLEMENTARY DATA

Tables S1 to S8 and Fig. S1 are given in supplementary data.

REFERENCES

[1] Fathalian, A.; Kanjouri, F.; Jalilian, J., BeO nanotube bundle as a gas sensor. *Super. Microstru.* **2013**, *60*, 291-299. DOI: org/10.1016/j.spmi.2013.04.028.

[2] Daniel, M. -C.; Astruc, D., Gold nanoparticles: assembly, supramolecular chemistry, quantum-size-related properties, and applications toward biology,

catalysis, and nanotechnology, *Chem. Rev.* **2004**, *104*, 293-346. DOI: 10.1021/cr030698.

[3] Zhang, Y.; Zhang, Y.; Zhang, D.; Liu, C., Novel chemical sensor for cyanides: boron-doped carbon nanotubes, *J. Phys. Chem. B.* **2006**, *110*, 4671-4674. DOI: 10.1021/jp0602272.

[4] Wang, R.; Zhang, D.; Zhang, Y.; Liu, C., Boron-doped carbon nanotubes serving as a novel chemical sensor for formaldehyde, *J. Phys. Chem. B.* **2006**, *110*, 18267-18271. DOI: 10.1021/jp061766.

[5] Wang, X.; Liew, K. M., Silicon carbide nanotubes serving as a highly sensitive gas chemical sensor for formaldehyde, *J. Phys. Chem. C.* **2011**, *115*,10388-10393. DOI: 10.1021/jp2005937.

[6] Field, C. R.; Yeom, J.; Salehi-Khojin, A.; Masel, R. I., Robust fabrication of selective and reversible polymer coated carbon nanotube-based gas sensors, *Sens. Actua. B. Chem.* **2010**, *148*, 315-322. DOI: 10.1016/j.snb.2010.05.026.

[7] Govind, N.; Andzelm, J.; Maiti, A., Dissociation chemistry of gas molecules on carbon nanotubes-applications to chemical sensing, *IEEE. Sens. J.* **2008**, *8*, 837-841. DOI: 10.1109/JSEN.2008.923947.

[8] Sousa, A. B.; Manzano, H.; Soto-Blanco, B.; Górniak, S. L., Toxicokinetics of cyanide in rats, pigs and goats after oral dosing with potassium cyanide, *Archiv. toxicology*. **2003**, *77*, 330-334. DOI: 10.1007/s00204-003-0446-y.

[9] Aitken, D.; West, D.; Smith, F.; Poznanski, W.; Cowan, J.; Hurtig, J.; Peterson, E.; Benoit, B., Cyanide toxicity following nitroprusside induced hypotension, *Canadian. Anaesth. Soc. J.* **1977**, *24*, 651-660. DOI: 10.1007/BF03006709.

[10] Marvi, M.; Raissi, H.; Ghiassi, H., Effects of the HCN adsorption on the structural and electronic parameters of the beryllium oxide nanotube, *Stru. Chem.* **2016**, *27*, 557-571. DOI: 10.1007/s11224-015-0585-9.

[11] Ansell, M.; Lewis, F., A review of cyanide concentrations found in human organs. A survey of literature concerning cyanide metabolism, 'normal', non-fatal, and fatal body cyanide levels, *J. Foren. Med.* **1969**, *17*, 148-155. DOI: 10.1017/BF03001702.

[12] Zhou, X.; Tian, W. Q., Sensitivity of (5,5) SWSiCNTs and SWSiCNTs with stone-wales defects toward hazardous molecules, *J. Phys. Chem. C.* **2011**, *115*, 11493-11499. DOI: 10.1021/jp2029196.

[13] Beheshtian, J.; Peyghan, A. A.; Bagheri, Z., Sensing behavior of Al-rich AlN nanotube toward hydrogen cyanide, *J. Mol. Mod.* **2013**, *19*, 2197-2203. DOI: org/10.1016/j.physleta.2017.01.010.

[14] Ahmadi Peyghan, A.; Hadipour, N. L.; Bagheri, Z., Effects of Al doping and double-antisite defect on the adsorption of HCN on a BC_2N nanotube: Density functional theory studies, *J. Phys. Chem. C.* **2013**, *117*, 2427-2432. DOI: org/10.1021/jp312503h.

[15] Srivastava, A.; Sharma, V.; Kaur, K., Khan, M. S.; Ahuja, R.; Rao, V., Electron transport properties of a single-walled carbon nanotube in the presence of hydrogen cyanide: first-principles analysis, *J. Mol. Mod.* **2015**, *21*, 1-7. DOI: 10.1007/s00894-015-2720-3.

[16] Sorokin, P.; Fedorov, A.; Chernozatonskiĭ, L., Structure and properties of BeO nanotubes, *Phys. Solid. State.* **2006**, *48*, 398-401. DOI: 10.1134/S106378340602034X.

[17] Baumeier, B.; Krüger, P.; Pollmann, J., Structural, elastic, and electronic properties of SiC, BN, and BeO nanotubes, *Phys. Rev. B.* **2007**, *76*, 085407. DOI: org/10.1103/PhysRevB.76.085407.

[18] Duman, S.; Sütlü, A.; Bağcı, S.; Tütüncü, H.; Srivastava, G., Structural, elastic, electronic and phonon properties of zinc-blende and wurtzite BeO, *J. Appl. Phys.* **2009**, *105*, 033719. DOI: org/10.1063/1.3075814.

[19] Gorbunova, M.; Shein, I.; Makurin, Y. N.; Ivanovskaya, V.; Kijko, V.; Ivanovskii, A., Electronic structure and magnetism in BeO nanotubes induced by boron, carbon and nitrogen doping, and beryllium and oxygen vacancies inside tube walls, *Physica E.* **2008**, *41*, 164-168. DOI: org/10.1016/j.physe.2008.07.002.

[20] He, J.; Wu, K.; Sa, R.; Li, Q.; Wei, Y., Modulating the electronic structures and optical absorption spectra of BeO nanotubes by uniaxial strain, *Appl. Phys. Let.* **2010**, *97*, 051901. DOI: org/10.1063/1.3473726.

[21] Seif, A.; Zahedi, E., A DFT studies of structural and quadrupole coupling constants properties in C-doped

BeO nanotubes, *Superl. Microstr.* **2011**, *50*, 539-548. DOI: org/10.1016/j.spmi.2011.08.016.

[22] Ma, L. -C.; Zhao, H. -S.; Yan, W. -J., Structural, electronic and magnetic properties of linear monoatomic chains adsorption on beryllium oxide nanotube: First-principle study, *J. Mag. Mag. Mater.* **2013**, *330*, 174-180. DOI: org/10.1016/j.jmmm.2012.11.001.

[23] Ahmadaghaei, N.; Noei, M., Density functional study on the sensing properties of nano-sized BeO tube toward H2S, *J. Iran. Chem. Soc.* **2014**, *11*, 725-731. DOI: org/10.1016/j.jmmm.2012.11.001.

[24] Rezaei-Sameti, M., The effects of SiC-doped on the NMR parameters of the armchair and zigzag models of aluminum phosphide nanotubes: A DFT study, *Physica E.* **2012**, *44*, 1770-1775. DOI: org/10.1016/j.physe.2011.12.016.

[25] Rezaei-Sameti, M., The effect of doping three Al and N atoms on the chemical shielding tensor parameters of the boron phosphide nanotubes: A DFT study, *Physica B.* **2012**, *407*, 22-26. DOI: org/10.1016/j.physb.2011.09.020.

[26] Rezaei-Sameti, M.; Jamil, E. S., The adsorption of CO molecule on pristine, As, B, BAs doped (4,4) armchair AlNNTs: a computational study, *J. Nanostr. Chem.* **2016**, 1-9. DOI: 10.1007/s40097-015-0183-9.

[27] Rezaei-Sameti, M.; Yaghoobi, S., Theoretical study of adsorption of CO gas on pristine and AsGa-doped (4,4) armchair models of BPNTs, *Comp. Condens. Mat.* **2015**, *3*, 21-29. DOI: org/10.1016/j.cocom.2015.01.001.

[28] Ditchfield, R.; Hehre, W. J.; Pople, J. A., Self-consistent molecular-orbital methods. IX. An extended Gaussian-type basis for molecular-orbital studies of organic molecules, *J. Chem. Phys.* **1971**, *54*, 724-728. DOI: org/10.1063/1.1674902.

[29] Schmidt, M. W.; Baldridge, K. K.; Boatz, J. A.; Elbert, S. T. ; Gordon, M. S.; Jensen, J. H.; Koseki, S.; Matsunaga, N.; Nguyen, K. A.; Su, S., General atomic and molecular electronic structure system, *J. Comp. Chem.* **1993**, *14*, 1347-1363. DOI: 10.1002/jcc.540141112.

[30] O'boyle, N. M.; Tenderholt, A. L.; Langner, K. M., A library for package-independent computational chemistry algorithms, *J. Com. Chem.* **2008**, *29*, 839-845. DOI: 10.1002/jcc.20823.

[31] Kim, D.; Bourée, J.; Kim, S., Numerical study on the field emission properties of aligned carbon nanotubes using the hybrid field enhancement scheme, *Appl. Phys. A.* **2006**, *83*, 111-114. DOI: 10.1007/s00339-005-3465-0.

[32] Stegmeier, S.; Fleischer, M.; Hauptmann, P., Influence of the morphology of platinum combined with β-Ga_2O_3 on the VOC response of work function type sensors, *Sensor. Actuat. B: Chem.* **2010**, *148*,439-449. DOI: org/10.1016/j.snb.2010.05.030.

[33] Peralta-Inga, Z.; Lane, P.; Murray, J. S.; Boyd, S.; Grice, M. E.; O'Connor, C. J.; Politzer, P., Characterization of surface electrostatic potentials of some (5,5) and (n,1) carbon and boron/nitrogen model nanotubes, *Nano Let.* **2003**, *3*, 21-28. DOI: 10.1021/nl020222q.

[34] Bulat, F. A.; Toro-Labbé, A.; Brinck, T.; Murray, J. S.; Politzer, P., Quantitative analysis of molecular surfaces: areas, volumes, electrostatic potentials and average local ionization energies, *J. Mol. Model.* **2010**, *16*, 1679-1691. DOI: 10.1007/s00894-010-0692-x.

[35] Bulat, F. A.; Burgess, J. S.; Matis, B. R.;. Baldwin, J. W.; Macaveiu, L.; Murray, J. S.; Politzer, P., Hydrogenation and fluorination of graphene models: analysis via the average local ionization energy, *J. Phys. Chem. A.* **2012**, *116*,8644-8652. DOI: 10.1021/jp3053604.

[36] James, C.; Raj, A. A.; Reghunathan, R.; Jayakumar, V.; Joe, I. H., Structural conformation and vibrational spectroscopic studies of 2,6-bis(p-N,N-dimethyl benzylidene) cyclohexanone using density functional theory, *J. Raman Spec.* **2006**, *37*, 1381-1392. DOI: 10.1002/jrs.1554.

[37] Keresztury, G. ; Holly, S.; Besenyei, G.; Varga, J.; Wang, A.; Durig, J., Vibrational spectra of monothiocarbamates-II. IR and Raman spectra, vibrational assignment, conformational analysis and ab initio calculations of S-methyl-N,N-dimethylthiocarbamate, *Spectrochimica Acta Part A: Molec. Spec.* **1993**, *49*, 2007-2026. DOI: org/10.1016/S0584-8539(09)91012-1.